frontiers in Materials

ORIGINAL RESEARCH
published: 13 December 2021
doi: 10.3389/fmats.2021.807900

Influence of Calcined Bauxite Aggregate on the Resistance of Cement Composites Subjected to Small Caliber Deformable Projectile Impact

Fengling Zhang[1] *and Rui Zhong*[2]*

[1]*Department of Civil and Environmental Engineering, National University of Singapore, Singapore, Singapore,* [2]*Engineering Research Center of Safety and Protection of Explosion and Impact of Ministry of Education, School of Civil Engineering, Southeast University, Nanjing, China*

This paper presents an experimental investigation on the influence of calcined bauxite aggregate (CBA) on the resistance of cement composites subjected to small caliber deformable projectile impact at a designed velocity of 400 m/s. The deformable projectile was made from copper with a purity of 99.5% and a diameter of 8.0 mm. Compared to mixtures with conventional coarse granite aggregate and/or siliceous fine aggregate, the incorporation of either fine or coarse CBA or their combination is beneficial in reducing the depth of penetration (DOP), equivalent crater diameter (CD), and crater volume (CV) caused by deformable projectile impact. CBA is found to be more effective in controlling the DOP and CV in comparison to the CD. Replacing of conventional aggregate with CBA leads to more severe damage to the projectiles (e.g., projectile length reduction, diameter increase, and mass loss). Relative effective hardness is an effective indicator to the deformation potential and penetration capacity of a deformable projectile to impact cement composites incorporating CBA.

Keywords: calcined bauxite, cement composites, projectile impact, penetration depth, crater

OPEN ACCESS

Edited by:
Kequan Yu,
Tongji University, China

Reviewed by:
Shaoqin Ruan,
Zhejiang University, China
Fei Zhou,
Tongji University, China

***Correspondence:**
Rui Zhong
cerzhong@seu.edu.cn

Specialty section:
This article was submitted to Structural Materials, a section of the journal Frontiers in Materials

Received: *02 November 2021*
Accepted: *19 November 2021*
Published: *13 December 2021*

Citation:
Zhang F and Zhong R (2021) Influence of Calcined Bauxite Aggregate on the Resistance of Cement Composites Subjected to Small Caliber Deformable Projectile Impact. Front. Mater. 8:807900. doi: 10.3389/fmats.2021.807900

INTRODUCTION

The resistance of cement composites subjected to extreme loadings, such as high-velocity projectile impact (HVPI), has been a research topic of much attention (Li et al., 2005; Zhang et al., 2005; Dancygier et al., 2007; Máca et al., 2014; Wu et al., 2015a; Kong et al., 2017; Zhang et al., 2021a; Zhang and Zhong, 2021; Zhong et al., 2021). It is increasingly recognized that besides compressive strength, the resistance of cement composites to HVPI is also significantly affected by aggregate (Yankelevsky, 2017). The experimental study by Zhang et al. (2005) reported that the inclusion of coarse granite aggregate (GA) into cement composites decreases the depth of penetration (DOP) as well as the equivalent crater diameter (CD). A similar phenomenon is also observed in (Werner et al., 2013; Wu et al., 2015b). Wu et al. (2015a) investigated the influence of coarse aggregate type (basalt and corundum), size (65–75 mm, 35–45 mm, and 5–20 mm), and volume fraction (45% and 30%). It was found that the use of stronger, harder, and larger size and higher volume fraction coarse aggregate is beneficial for the resistance of concrete subjected to HVPI. The positive influence of coarse aggregate is also confirmed in (Dancygier and Yankelevsky, 1999; Bludau et al., 2006; Dancygier et al., 2007;

TABLE 1 | Physical and mechanical properties of GA and CBA.

Type	Crushing value	Elastic modulus	Compressive strength	Specific gravity	Hardness
GA	32.7%	65.0 GPa	238.5 MPa	2.65	21.1 HRC, 93.7 HR15T
CBA	8.0%	240.0 GPa	N.A.	3.20	51.6 HRC, 96.7 HR15T

Note: The aggregate crushing value was determined according to BS 812–110 (British Standards BS 812-110, 1990). The elastic modulus was measured using Ø75 × 130-mm cylindrical specimen for GA whereas it was estimated using $E = [V^2\rho(1+\nu)(1-2\nu)]/(1-\nu)$ for CBA where V, ρ and ν are the velocity of ultrasonic pulse, density and Poisson's ratio of CBA, respectively. The compressive strength was determined using Ø75 × 130-mm cylindrical specimen for GA and is not available for CBA owing to the difficulties in obtaining sufficiently large test specimen. The specific gravity was determined according to ASTM C127 (ASTM C127, 2015). The hardness was measured based on HRC and HR15T scales, respectively, according to the procedures described in (Zhang et al., 2020b).

TABLE 2 | The mixture proportions of cement composites.

Mixture designation		*w/b*	Fine aggregate (sand)	Coarse aggregate	Mixture proportions (kg/m^3)						
					Water	Cement	Silica fume	Fine aggregate (sand)	Coarse aggregate	Steel fiber	Superplasticizer
Mortar	M-0.60-S	0.60	Siliceous	—	330	549	—	1288	—	39 (0.5% by volume)	0
	M-0.28-S	0.28			231	751	75	1288	—		4.3
	M-0.17-S	0.17			168	901	90	1288	—		12.7
	M-0.60-B	0.60	Bauxite	—	330	549	–	1567	—		0
	M-0.28-B	0.28			231	751	75	1567	—		3.6
	M-0.17-B	0.17			168	901	90	1567	—		15.9
Concrete	C-0.28-SG	0.28	Siliceous	Granite	139	450	45	772	946	39 (0.5% by volume)	10.0
	C-0.28-SB	0.28		Bauxite	139	450	45	772	1142		6.0
	C-0.28-BB	0.28	Bauxite	Bauxite	139	450	45	939	1142		5.7

Wu et al., 2015b; Wang et al., 2016; Zhong et al., 2021). Apart from coarse aggregate, the inclusion of siliceous fine aggregate into cement composites could also lead to improved resistance to some extent such as decreasing the DOP (Dancygier et al., 2007; Wang et al., 2016; Zhong et al., 2021). A recent study by Wang et al. (2016) found that the DOP appears to reduce with the increase of effective hardness which is calculated based on the hardness and volume proportion of matrix and coarse aggregate.

Zhang et al. (2020a) investigated the HVPI resistance of cement composites characterized with a wide range of compositions and compressive strengths ranging from 34.2 to 220.2 MPa. It was identified that the effective hardness is a critical parameter governing the DOP since it characterizes the overall contribution of fine and coarse aggregate as well as matrix. Zhong et al. (2021) compared the HVPI resistance of a variety of advanced concretes, including ultra-high performance concrete (UHPC), fiber reinforced high strength concrete (FRHSC) and engineered cementitious composites (ECC). In contrast to the relatively small projectiles used in (Zhang et al., 2020a), sufficiently large caliber projectiles were used to avoid potentially biased results due to the presence of coarse aggregate. The beneficial effect of coarse aggregate was observed and a close correlation between the effective hardness and DOP was identified. To sum up, the incorporation of aggregate is beneficial for the resistance of cement composites to HVPI. However, these studies focused on the performance of cement composites subjected to non-deformable projectile impact.

Due to its high strength and hardness [compressive strength in excess of 2000 MPa and Moh's hardness of approximately 9.5 (Wu et al., 2015a)], the use of calcined bauxite aggregate (CBA) in cement composites indeed resulted in substantially improved mechanical properties and resistance to HVPI as reported in our earlier work (Zhang et al., 2021b). Nevertheless, non-deformable projectiles were used in that study. The effect of CBA on the resistance of cement composites subjected to HVPI using deformable projectile is not clear. However, there are practical issues warranting a better understanding of such effect. Aircraft engine missile attack is an important concern in the design of nuclear power plant containments, skyscrapers and critical bridges as pointed by Kœchlin and Potapov (2009). The aircraft engine missile can be equivalently treated as a deformable projectile in these cases as reported in (Kœchlin and Potapov, 2009; Riedel et al., 2010; Zhang et al., 2018).

In contrast to the extensive investigations on the behavior of cement composites subjected to non-deformable HVPI, only a limited number of experimental studies are devoted to deformable HVPI (Gold et al., 1996; Nia et al., 2014; Kong et al., 2017; Feng et al., 2018). Furthermore, among those limited studies, focus was placed on the influence of striking velocity. Kong et al. (2017) explored the influence of striking velocities ranging from 510 to 1850 m/s and observed three penetration regimes with increasing impact velocities: rigid penetration, deformable penetration without eroding, and eroding penetration regimes. To the best knowledge of the

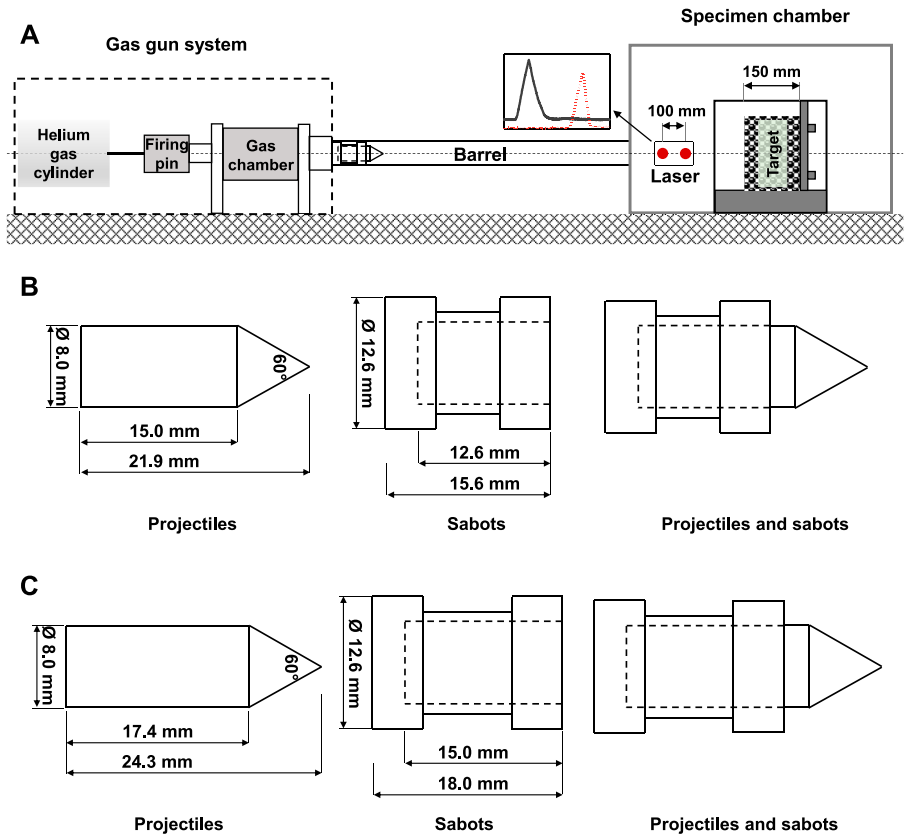

FIGURE 1 | Schematic of **(A)** HVPI test setup, **(B)** copper, and **(C)** steel projectile and their sabot.

TABLE 3 | Properties of copper and steel used for different projectiles.

Type	Yield strength[a]	Ultimate strength[a]	Elastic modulus[a]	Poisson's ratio[a]	Density[a]	Hardness
Copper	275 MPa	290 MPa	115 GPa	0.34	8,940 kg/m^3	~42 HRB[a], 78.4 HR15T[b]
Steel	2150–2200 MPa	2950–3100 MPa	210 GPa	0.30	7,700 kg/m^3	60–62 HRC[a], 97.2 HR15T[b]

[a]*Provided ay the supplier.*
[b]*Determineb in our laboratory.*

authors, the influence of coarse aggregate on cement composites subjected to deformable HVPI is far from well understood and relevant experimental studies are rarely reported.

This study is a continuation of our earlier work to unveil the influence of CBA (both fine and coarse) on the resistance of cement composites subjected to the impact of deformable projectiles. The cement composites investigated in this study include six mortars and three concretes with unconfined Ø100 × 200-mm cylindrical compressive strengths ranging from 37.9 to 210.2 MPa. The dimension of the specimens for the HVPI test is 300 × 170 × 150-mm. Conical-nosed deformable projectiles were made from copper weighting 7.8 g and with a diameter of 8.0 mm. The designed striking velocity is 400 m/s.

The damage of cement composites induced by the HVPI is quantified based on the depth of penetration (DOP), equivalent crater diameter (CD), and crater volume (CV), while the damage of projectiles is characterized based on the length reduction (γ_l), diameter increase (γ_d), and mass loss (γ_m). The results of our earlier work (Zhang et al., 2021b), where the same array of cement composites, impacted by non-deformable projectiles having the same mass, diameter, and target striking velocity, are also included for comparison purpose.

MATERIAL AND METHODS

Materials

CBA utilized in this study possesses an 83.4% aluminium oxide (Al_2O_3) content and a specific gravity of 3.20. Conventional aggregates utilized include siliceous fine aggregate with a fineness modulus of 2.70 and a specific gravity of 2.63, as well as coarse granite aggregate (GA) with a specific gravity of 2.65 and a maximum aggregate size of 10 mm. **Table 1** compares the physical and mechanical properties of the coarse CBA and GA.

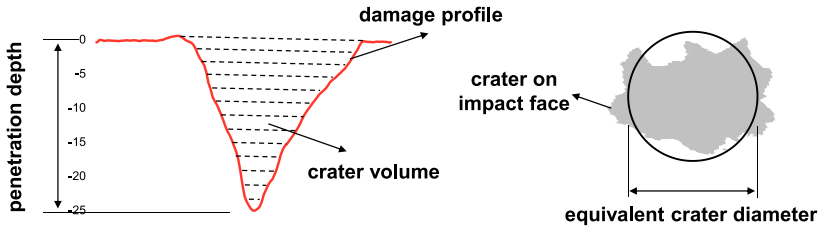

FIGURE 2 | Illustration on the measurement of DOP, CD, and CV.

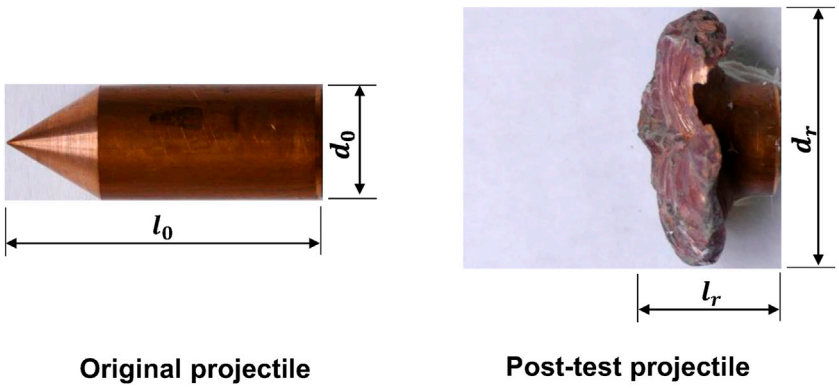

FIGURE 3 | Original and residual length and diameter measurement of a copper projectile.

Based on the significantly lower aggregate crushing value (32.7% vs. 8.0% for GA and CBA, respectively), which is defined as the percentage by weight of the crushed material obtained when the aggregates are subjected to a specific load (British Standards BS 812-110, 1990), it is reasonable to assume that the compressive strength of GA is lower compared to that of CBA. In addition, the CBA exhibits both higher hardness and elastic modulus than that of the GA (**Table 1**). Detailed comparisons between these two aggregates can be found in our earlier work (Zhang et al., 2021b). To minimize the effect of aggregate gradation, as-received CBAs were sieved and tailored to achieve similar particle size distributions as conventional aggregates. CEM I 52.5N ordinary Portland cement was utilized for all mixtures. Microsilica Grade 940U silica fume from Elkem was utilized. Steel fibers were provided by Bekaert with a diameter of 0.16 mm and a length of 13 mm. ADVA 181N polycarboxylate-based superplasticizer supplied by GCP Applied Technologies was utilized in some mixtures for workability improvement purpose.

Mixture Design and Specimen Preparation

Table 2 provides the mixture proportions of all mixtures investigated in this study. The water to binder (*w/b*) ratio was varied from 0.17 to 0.60 to achieve different compressive strength levels. The designation of mixtures starts with a letter followed by a numerical number. The letters M and C represent mortar and concrete, respectively. The following number indicates the *w/b* ratio. The mixture designation ends with one or two letters for the type of used aggregate. For mortars, no coarse aggregate is used and thus there is only one ending letter. S and B stand for siliceous sand and fine CBA, respectively. For concretes, there are two ending letters with the first and the second letters indicate the type of fine and coarse aggregate, respectively. For example, C-0.28-SG means the concrete mixture has a *w/b* ratio of 0.28 and both siliceous sand and coarse GA are used. All of the cement composites incorporated a 0.5% volume fraction of steel fibers in order to alleviate the specimen splitting after the HVPI tests and to facilitate a consistent damage characteristics measurement (Zhang et al., 2021b). A Hobart mixer was utilized for mixing mortars and a pan mixer was utilized for mixing concretes. Dry materials (cement, silica fume, fine or coarse aggregate) were firstly dry-mixed for 1–2 min, followed by the addition of water (Cai et al., 2021). A proper amount of superplasticizer was then added to improve the workability of mortar and concrete mixtures. Lastly, steel fibers were added by hand once the mixture turned fluid. All the specimens were covered with plastic sheets and left in laboratory after casting, demolded after 1 day and stored in a fog room for additional 6 days. Thereafter, all the specimens were left in the laboratory at an ambient temperature of approximately 30°C until testing at an age of around 91 days.

Test Methods

At the age of HVPI tests, the compressive strengths and elastic moduli of different mixtures were determined using Ø100 × 200-mm cylindrical specimens following the ASTM C39 (ASTM C39, 2017) and ASTM C469 (ASTM C469, 2014), respectively. The Rockwell hardness was measured using 100-mm length cubic

TABLE 4 | Summary of the DOP, CD, and CV in cement composites subjected to copper and steel projectile impact.

Mixture		w/b	Fine aggregate (sand)	Coarse aggregate	Compressive strength (MPa)	Elastic modulus (GPa)	Effective hardness (HR15T)	Copper projectile impact						Steel projectile impact					
								Type of projectile damage	Striking velocity (m/s)	DOP (mm)	Normalized DOP ($\times10^{-3}$ mm/(m/s))	CD (mm)	CV ($\times10^{-1}$ ml)	Type of projectile damage	Striking velocity (m/s)	DOP (mm)	Normalized DOP ($\times10^{-3}$ mm/(m/s))	CD (mm)	CV ($\times10^{-1}$ ml)
Mortars	M-0.60-S	0.60	Siliceous	—	37.9±0.2	21.5±0.7	46.2	Deformable	395.1±15.6	19.7±2.6	49.6±4.6	66.9±5.5	130.3±27.8	Non-deformable	412.3±10.5	30.8±1.5	74.6±1.7	66.2±6.3	122.3±24.8
	M-0.28-S	0.28			93.4±1.4	36.7±0.4	69.3	Deformable	403.2±0.0	10.0±1.2	24.8±2.9	48.8±0.4	48.3±4.5	Non-deformable	396.8±0.0	15.8±0.7	39.7±1.8	59.3±2.2	79.0±4.6
	M-0.17-S	0.17			146.9±1.4	49.5±0.7	76.2	Deformable	410.1±12.0	6.6±1.4	16.0±3.1	40.4±5.9	23.3±9.8	Non-deformable	409.2±11.0	12.4±1.1	30.2±1.9	55.8±2.7	68.0±13.1
	M-0.60-B	0.60	Bauxite	—	45.0±0.3	30.1±0.5	50.1	Deformable	427.4±3.7	18.3±1.8	42.8±3.9	56.2±3.5	61.3±13.7	Non-deformable	426.1±2.1	27.6±2.1	64.8±4.8	60.7±3.2	99.0±5.0
	M-0.28-B	0.28			120.0±2.4	56.8±1.2	74.2	Deformable	431.1±3.7	8.5±0.9	19.6±1.9	44.9±0.8	42.7±7.6	Non-deformable	420.3±9.2	12.7±0.9	30.1±1.4	53.9±1.5	64.3±8.7
	M-0.17-B	0.17			190.9±3.4	77.7±2.1	80.0	Deformable	405.5±8.2	3.9±0.7	9.6±1.5	26.4±1.2	12.3±1.5	Non-deformable	425.6±4.7	11.6±1.6	27.1±3.4	51.8±5.9	59.8±19.5
Concretes	C-0.28-SG	0.28	Siliceous	Granite	118.1±3.4	46.7±0.2	80.2	Deformable	409.0±4.2	7.6±0.3	18.6±0.6	41.7±3.9	24.3±7.6	Non-deformable	411.2±11.8	11.2±2.9	27.1±6.1	50.4±5.4	55.3±8.8
	C-0.28-SB	0.28		Bauxite	156.0±6.7	82.3±3.0	85.6	Deformable	425.6±7.0	5.4±1.3	12.7±2.8	36.5±2.9	20.5±11.8	Deformable	426.8±4.8	10.4±2.2	24.3±5.0	52.1±2.9	54.8±7.2
	C-0.28-BB	0.28	Bauxite	Bauxite	210.2±2.2	108.8±0.5	87.0	Deformable	427.4±4.2	3.9±1.0	9.0±2.4	26.7±2.6	6.3±3.3	Deformable	431.0±2.4	8.7±1.8	20.2±4.1	49.2±5.8	44.2±14.4

Note that 1) DOP is the depth of penetration, CD is the equivalent crater diameter, CV is the crater volume, and 2) experimental results are expressed as average value ± standard deviation as at least three specimens are tested for each mixture.

TABLE 5 | Summary of the γ_l, γ_d, and γ_m of copper and steel projectiles after HVPI tests.

Mixture		w/b	Fine aggregate (sand)	Coarse aggregate	Compressive strength (MPa)	Copper projectile impact					Steel projectile impact				
						Type of projectile damage	Striking velocity (m/s)	Normalized γ_l ($\times10^{-5}$/(m/s))	Normalized γ_d ($\times10^{-5}$/(m/s))	Normalized γ_m ($\times10^{-5}$/(m/s))	Type of projectile damage	Striking velocity (m/s)	Normalized γ_l ($\times10^{-5}$/(m/s))	Normalized γ_d ($\times10^{-5}$/(m/s))	Normalized γ_m ($\times10^{-5}$/(m/s))
Mortars	M-0.60-S	0.60	Siliceous	—	37.9±0.2	Deformable	395.1±15.6	12.5±2.9	17.7±1.7	1.3±0.1	Non-deformable	412.3±10.5	—	—	—
	M-0.28-S	0.28			93.4±1.4	Deformable	403.2±0.0	56.3±11.4	90.3±4.5	1.6±0.2	Non-deformable	396.8±0.0	2.3±0.8	0.0±0.0	1.1±0.0
	M-0.17-S	0.17			146.9±1.4	Deformable	410.1±12.0	110.9±15.5	231.2±37.4	1.8±0.1	Non-deformable	409.2±11.0	4.1±1.4	0.0±0.0	1.3±0.1
	M-0.60-B	0.60	Bauxite	—	45.0±0.3	Deformable	427.4±3.7	38.6±0.2	66.7±2.1	1.5±0.3	Non-deformable	426.1±2.1	—	—	—
	M-0.28-B	0.28			120.0±2.4	Deformable	431.1±3.7	96.4±19.6	201.4±11.6	1.9±0.2	Non-deformable	420.3±9.2	3.7±1.6	0.0±0.0	1.6±0.1
	M-0.17-B	0.17			190.9±3.4	Deformable	405.5±8.2	146.9±22.6	388.5±18.1	5.9±0.1	Non-deformable	425.6±4.7	6.0±0.9	0.0±0.0	1.7±0.2
Concretes	C-0.28-SG	0.28	Siliceous	Granite	118.1±3.4	Deformable	409.0±4.2	92.6±17.4	246.8±7.2	2.3±0.2	Non-deformable	411.2±11.8	4.5±1.6	0.0±0.0	1.1±0.1
	C-0.28-SB	0.28	Siliceous	Bauxite	156.0±6.7	Deformable	425.6±7.0	109.0±9.9	301.9±22.4	3.7±1.9	Deformable	426.8±4.8	17.5±2.6	0.0±0.0	5.6±1.1
	C-0.28-BB	0.28	Bauxite	Bauxite	210.2±2.2	Deformable	427.4±4.2	147.3±24.7	400.8±15.6	7.6±1.2	Deformable	431.0±2.4	25.1±3.4	0.0±0.0	9.4±1.3

Note that 1) γ_l is the projectile length reduction, γ_d is the projectile diameter increase, γ_m is the projectile mass loss, and 2) experimental results are expressed as average value ± standard deviation as at least three specimens are tested for each mixture.

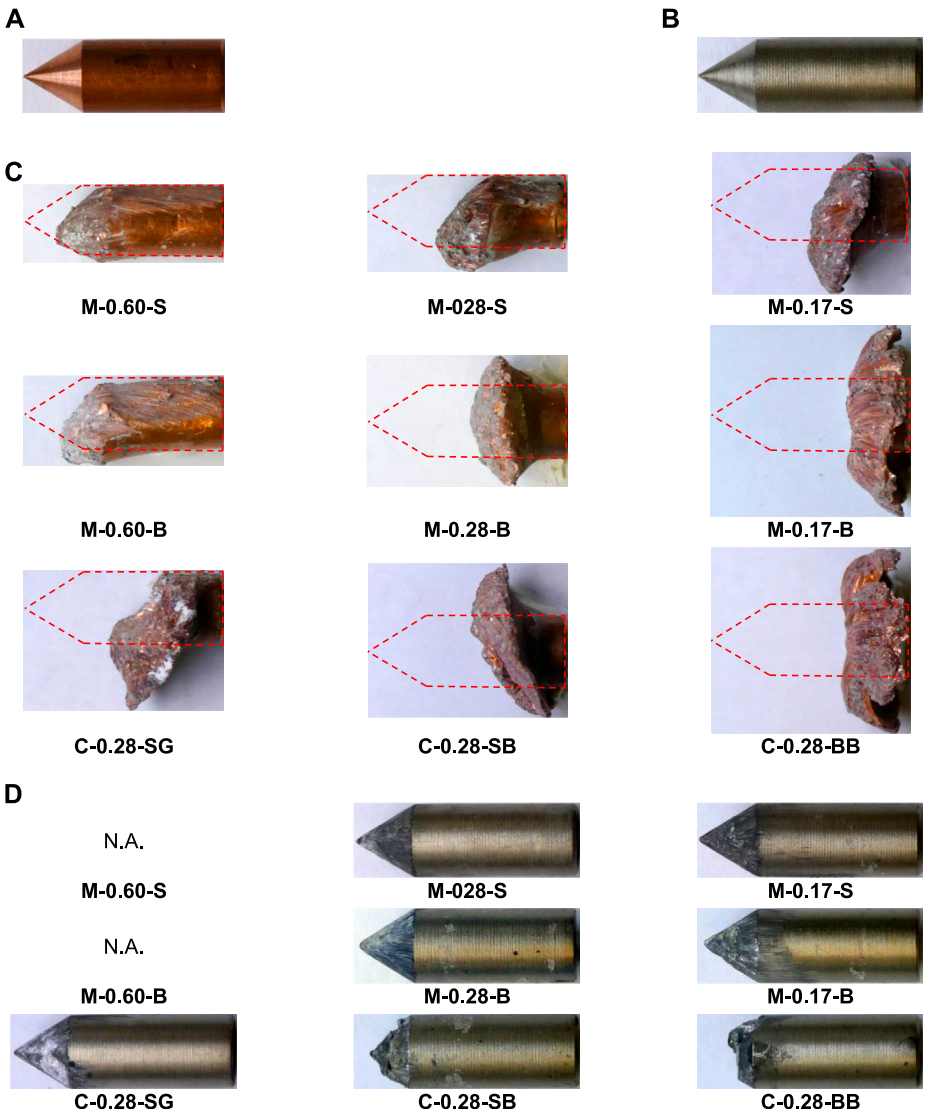

FIGURE 4 | Images of **(A)** original copper projectile, **(B)** original steel projectile, **(C)** post-HVPI test copper projectiles, and **(D)** post-HVPI test steel projectiles..

specimens with HR15T scale following (Wang et al., 2016; Zhang et al., 2020a; Zhang et al., 2020b). Since the typical depth of indentation in a hardness test is smaller than 1 mm, an effective hardness was proposed as an overall characterization of a cement composite's hardness (Wang et al., 2016). It can be calculated using **Eq. 1** as defined below.

$$H_{eff} = \frac{l_{ca}}{l_{ca}+l_m}H_{ca} + \frac{l_m}{l_{ca}+l_m}H_m \qquad (1)$$
$$l_m = \sqrt[3]{V_m},\ l_{ca} = \sqrt[3]{V_{ca}}$$

where H_m and H_{ca} are the measured hardness values of mortar and coarse aggregate, respectively; l_m and l_{ca} are the equivalent lengths of mortar and aggregate, respectively; V_m and V_{ca} are the volume fractions of mortar and coarse aggregate, respectively. More details regarding the effective hardness can be found in Wang et al. (2016). Note that for mortars without coarse aggregate, their effective hardness indices are equal to the measured hardness values.

HVPI tests were conducted using a light gas gun as shown in **Figure 1A**. A 300 × 170 × 150-mm block was placed in a steel jip and aligned such that a projectile would strike perpendicularly against the center of the front surface of each specimen. A pair of laser sensors was set up to determine the actual striking velocity of a projectile. Conical nosed projectiles weighting 7.9 g with a diameter of 8 mm were used. In contrast to the ASSAB XW-42 steel used in our previous work (Zhang et al., 2021b), copper with a purity of 99.5% was selected for the deformable projectile based on a series of preliminary studies. The properties of 99.5% copper and ASSAB XW-42 steel are provided in **Table 3**. Considering the higher density of copper (8,940 kg/m^3) compared with steel (7,700 kg/m^3), a slightly shorter shank

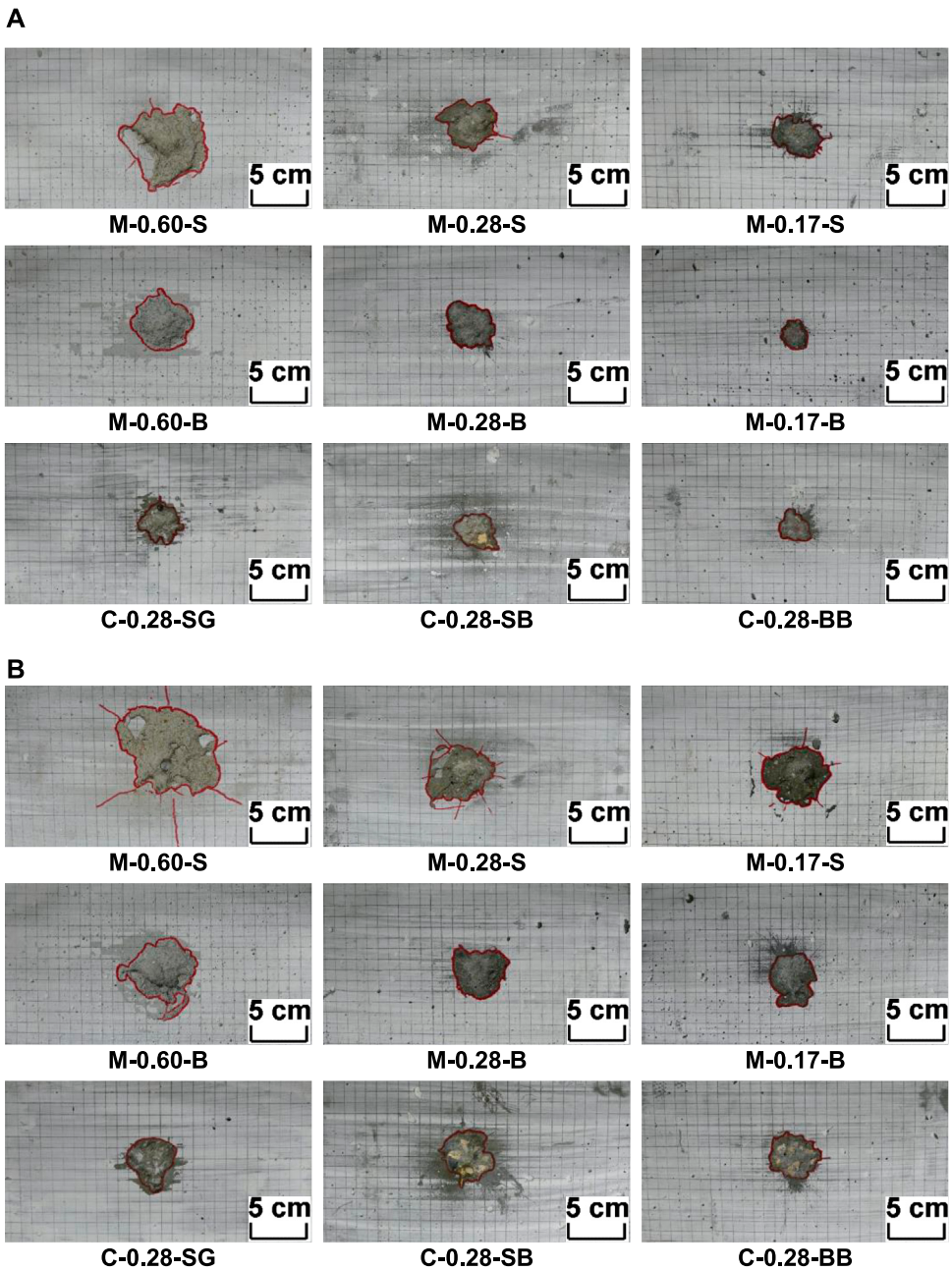

FIGURE 5 | Damage of cement composites after impact tests **(A)** deformable projectile and **(B)** non-deformable projectile.

length for the copper projectile was designed to ensure the same initial impact energy (**Figures 1B** and **C**). It should be noted that such slight difference in projectile length has a negligible influence on the performance of cement composites subjected to HVPI (Li et al., 2005). A polypropylene plastic sabot weighting 1.7 g was attached to the projectile to ensure a proper fit into the 12.7 mm barrel of the light gas gun. Compressed helium gas was utilized to propel the projectile at the pressure of approximately 35 bar to achieve the designed striking velocity of 400 m/s. The HVPI tests were conducted at an age of approximately 91 days. A set of new projectile, sabot, and specimen was utilized for each HVPI test.

The damage to the cement composites induced by the HVPI was quantified based on the depth of penetration (DOP), equivalent crater diameter (CD), and crater volume (CV), as illustrated in **Figure 2**. DOP is the distance from the impact face to the deepest point of a crater. CD is the diameter of an equivalent circle possessing an identical area with the spalling crater, which was determined by counting the 10 × 10-mm grids drew on the front face prior to HVPI test. CV is determined as the

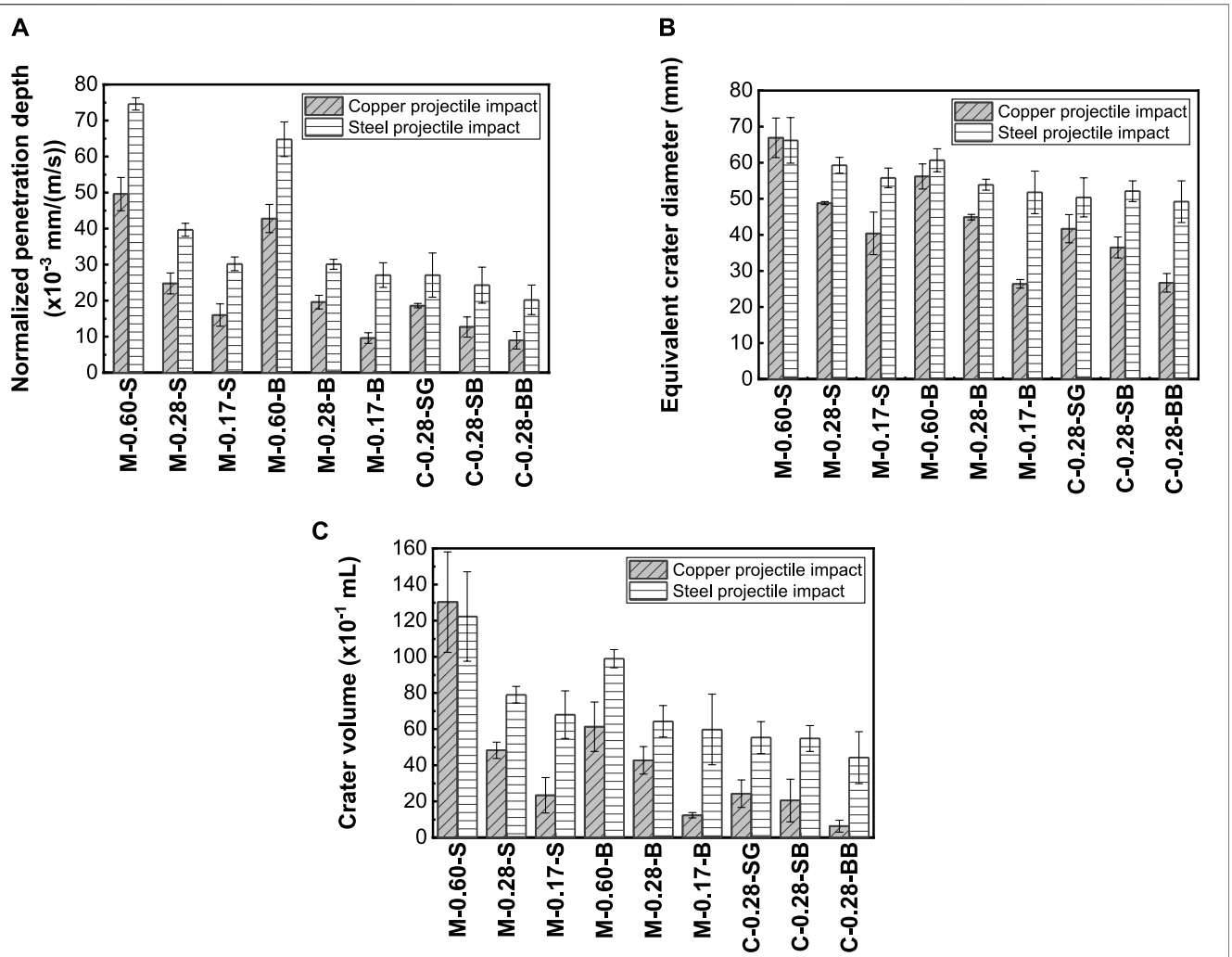

FIGURE 6 | Comparison of the normalized damage characteristics of cement composites, **(A)** DOP, **(B)** CD, and **(C)** CV.

sand volume needed to fill up a crater. The constituent (mortar or coarse aggregate) upon which the projectile struck against influences the characteristics of corresponding damage. To minimize the variation of experimental results because of the relatively small diameter of projectile, three and four replicates were tested for the mortar and concrete mixtures, respectively. Note that the practical limitation of small projectile size was also recognized in (Gold et al., 1996; Gomez and Shukla, 2001; Zhang et al., 2005; Bludau et al., 2006; Werner et al., 2013; Máca et al., 2014; Nia et al., 2014; Wu et al., 2015a; Peng et al., 2016; Song et al., 2019). In total, thirty 300 × 170 × 150-mm specimens were tested. The average values together with corresponding standard deviations are reported.

The damage to the projectiles was characterized by its change of length (γ_l), diameter (γ_d), and mass (γ_m) following (Xiao et al., 2010; Kong et al., 2017; Zhang et al., 2020b), and can be calculated using **Eqs 2–4**, respectively, as defined below.

$$\gamma_l = |(l_0 - l_r)/l_0| \tag{2}$$

$$\gamma_d = |(d_0 - d_r)/d_0| \tag{3}$$

$$\gamma_m = |(m_0 - m_r)/m_0| \tag{4}$$

where l_0 and l_r are the original and residual projectile lengths, respectively; d_0 and d_r are the original and residual projectile diameters, respectively; m_0 and m_r are the original and residual projectile masses, respectively. An example on the measurement of original and residual projectile lengths and diameters is illustrated in **Figure 3**.

RESULTS AND DISCUSSION

Influence of Deformable Nature of Projectile on the Damage Characteristics of Cement Composites

The damage characteristics of cement composites and projectiles after HVPI tests are summarized in **Tables 4** and **5**, respectively. Note that

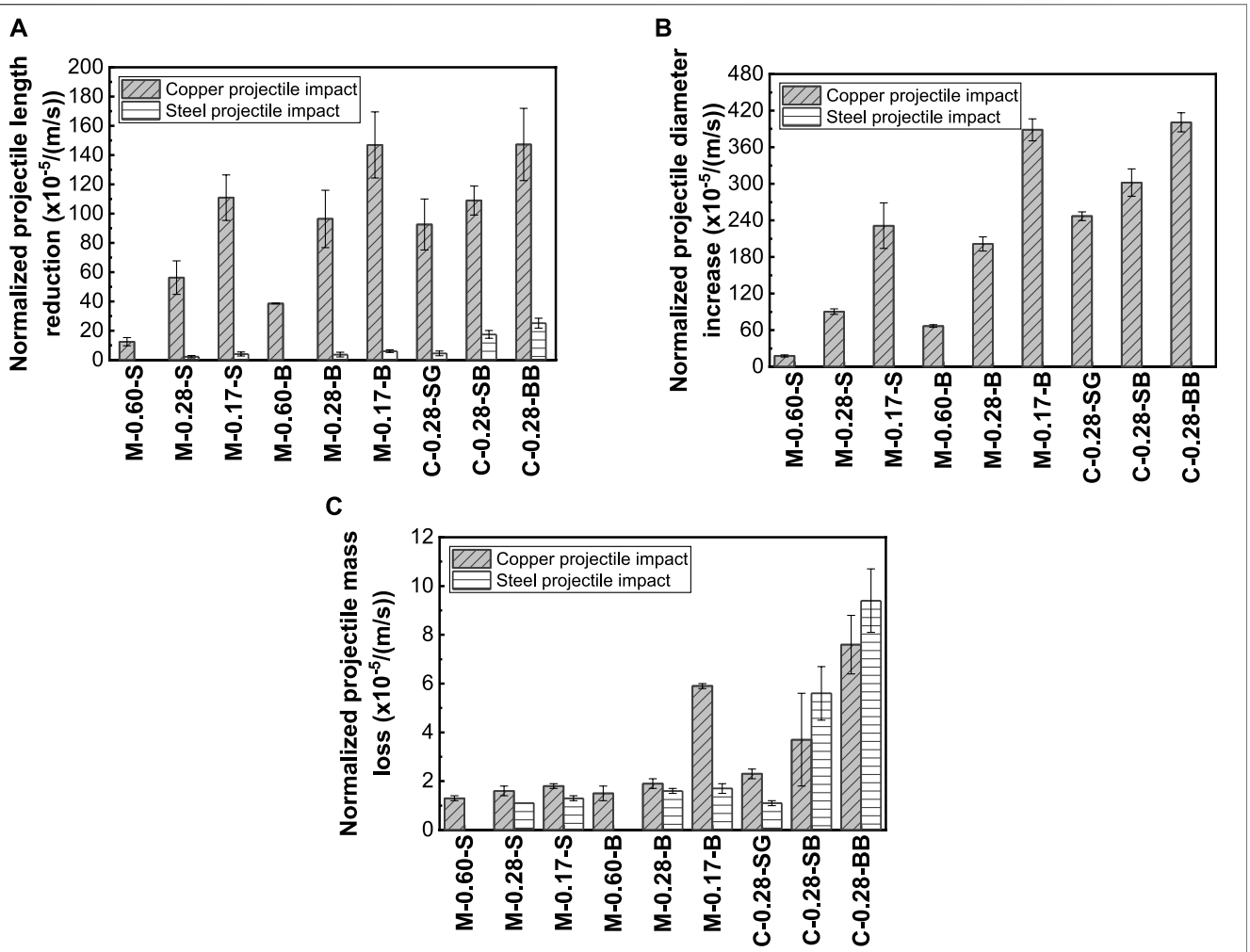

FIGURE 7 | Comparison of the normalized damage characteristic of projectiles, **(A)** length reduction, **(B)** diameter increase, and **(C)** mass loss.

the results of our earlier work (Zhang et al., 2021b) using steel projectiles are also included for comparison purpose. The test conditions in this study and that earlier work (Zhang et al., 2021b) are essentially the same such as the projectile nose shape (conical), mass (7.8 g), diameter (8.0 mm), striking velocity (approximately 400 m/s), and specimen dimension (300 × 170 × 150-mm). There is a slight difference in the projectile length due to the difference in densities of copper and steel (see *Test Methods*). The major difference lies in the nature of projectiles. **Figure 4** presents the original and post-HVPI test images of the projectiles which indicates the deformable and non-deformable nature of copper and steel projectiles, respectively. Substantial length reduction, diameter increase, and mass loss occurred for all the copper projectiles whereas the steel projectiles essentially maintained the original conditions except for minor scratch or deformation. It is worth pointing out that the steel projectiles impacting C-0.28-SB and C-0.28-BB also demonstrated appreciable deformation and damage which is most likely due to the direct collision with coarse CBA. However, for simplicity, copper and steel projectiles will be referred to as deformable and non-deformable projectiles in the following analyses and discussions. The steel projectiles striking against M-0.60-S and M-0.60-B were fully embedded in the targets and thus were not retrieved. Therefore, these images are not available.

The measured striking velocities varied between 380 and 435 m/s, although the designed striking velocity was set as 400 m/s. The slight difference in actual striking velocities may affect the corresponding damage characteristics. Indeed, the experimental study by Zhang et al. (2005) found a linear relationship between the DOPs and projectile striking velocities ranging from 250 to 650 m/s. In contrast, the CDs and CVs appeared unaffected by the striking velocities. This is consistent with those reported in (Maalej et al., 2005; Feng et al., 2018). Therefore, the DOPs are normalized with respect to the striking velocities in the following analyses and discussions, but the CDs and CVs are not adjusted. Normalization was also conducted when assessing the projectile length reduction, diameter increase, and mass loss for the same reason (Zhang et al., 2020b). The post-HVPI test images of cement composites subjected to the deformable and non-deformable projectiles are provided in

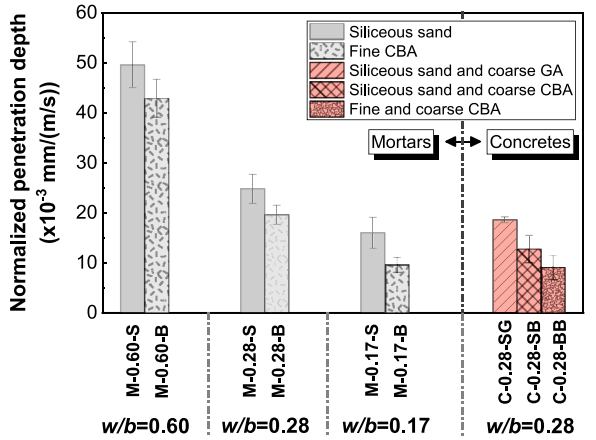

FIGURE 8 | Effect of CBA on the DOP of cement composites subjected to deformable copper HVPI.

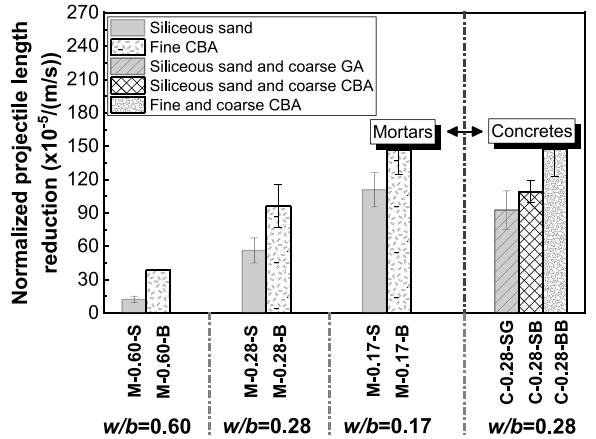

FIGURE 9 | Effect of CBA on the normalized length reduction of deformable copper projectile.

Figure 5. It can be observed that the damage of cement composites is largely localized and neither scabbing nor perforation is observed.

Figure 6 compares the damage characteristics of investigated cement composites. It is observed that for the same target under the given set of impact conditions, the DOPs, CDs, and CVs resulting from the impact of deformable (copper) projectiles are much smaller than those caused by the impact of non-deformable (steel) projectiles. **Figure 7** shows the damage characteristics of investigated projectiles. The length reduction, diameter increase, and mass loss of deformable (copper) projectiles after the HVPI tests are significantly greater compared to those of non-deformable (steel) projectiles under similar impact conditions. When a projectile deforms during HVPI, part of the kinetic energy is consumed by its deformation and less kinetic energy will be available for the penetration process (Ohno et al., 1992). For a given impact condition, the larger the projectile deformation, the less severe the damage caused by the projectile. This explains the smaller DOPs, CDs, and CVs resulting from the impact of deformable (copper) projectiles compared to that caused by the non-deformable (steel) projectiles.

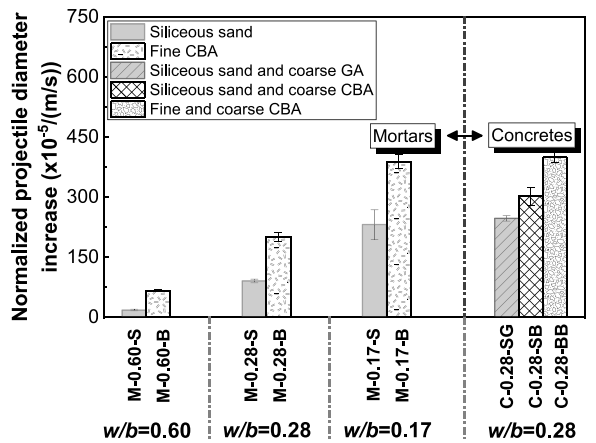

FIGURE 10 | Effect of CBA on the normalized diameter increase of deformable copper projectile.

Effect of CBA on the Damage Characteristics of Cement Composites

Effect of CBA on the Depth of Penetration

It can be observed from **Figure 8** that when subjected to deformable HVPI, the inclusion of fine CBA in mortars (M-0.60-B, M-0.28-B, and M-0.17-B) decreases the DOPs by 14–40% in comparison to the counterparts using siliceous sand (M-0.60-S, M-0.28-S, and M-0.17-S). The inclusion of coarse CBA in concrete (C-0.28-SB) leads to a 32% decrease of the DOP compared with that using coarse GA (C-0.28-SG). These observations clearly demonstrate that replacing the conventional aggregates (siliceous sand or coarse GA) with CBA (either fine or coarse) is beneficial for reducing the DOP. In addition, the mixed use of coarse and fine CBA (C-0.28-BB) exhibits a further DOP reduction of 52% and 30% compared to that containing no CBA (C-0.28-SG) or coarse CBA only (C-0.28-SB), respectively.

The stress in a specimen subjected to HVPI increases rapidly, which drives a large number of micro-cracks into rapid propagation. In contrast to the quasi-static loading in which sufficient time is allowed for micro-cracks to seek the path of least resistance [e.g., interfacial transition zone between aggregate and matrix (Wu et al., 2020a)], the micro-cracks under impact loading are generally forced to propagate directly through the aggregate particles, instead of the weaker phase such as interfacial transition zone (Zielinski, 1984; Bischoff and Perry, 1991; Zhang et al., 2005; Wang et al., 2016; Wu et al., 2020a; Wu et al., 2020b; Zhong et al., 2021; Zhang et al., 2021a; Wu et al., 2021). Since the compressive strength of CBA is considerably higher than that of GA [more than 2000 MPa for CBA as reported in (Wu et al., 2015a) vs. 238.5 MPa for GA as given in **Table 1**], it thus has better capability of arresting

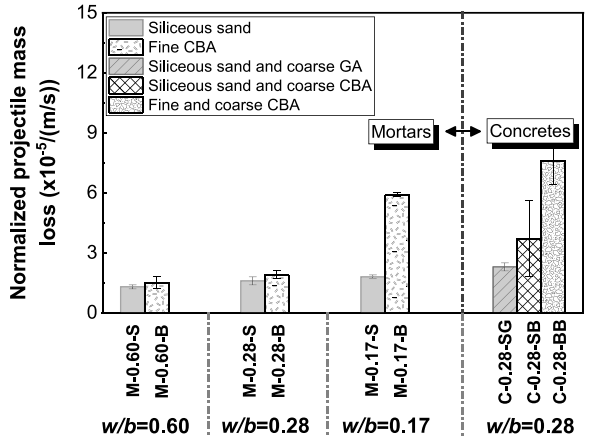

FIGURE 11 | Effect of CBA on the normalized mass loss of deformable copper projectile.

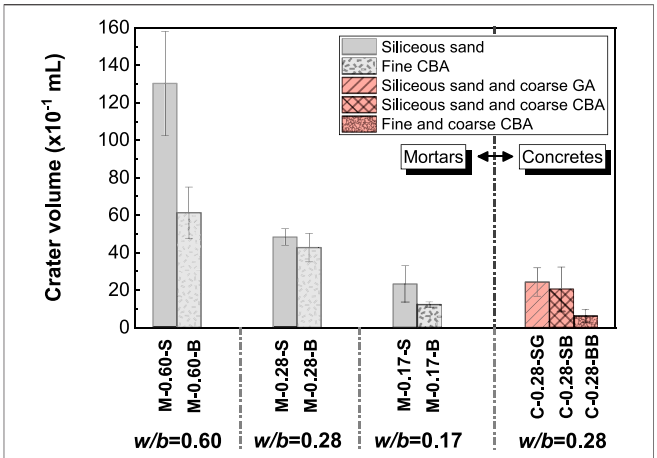

FIGURE 13 | Effect of CBA on the CV of cement composites subjected to deformable copper HVPI.

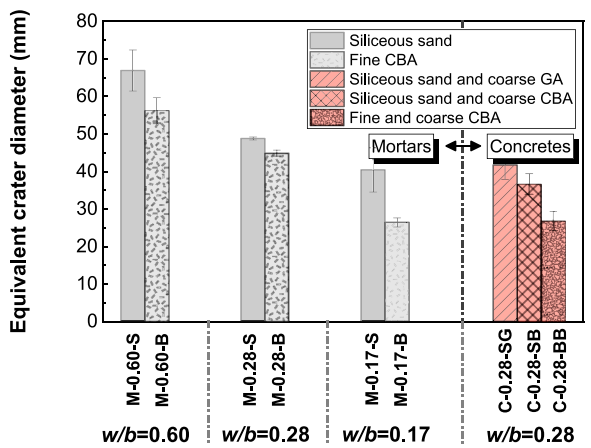

FIGURE 12 | Effect of CBA on the CD of cement composites subjected to deformable copper HVPI.

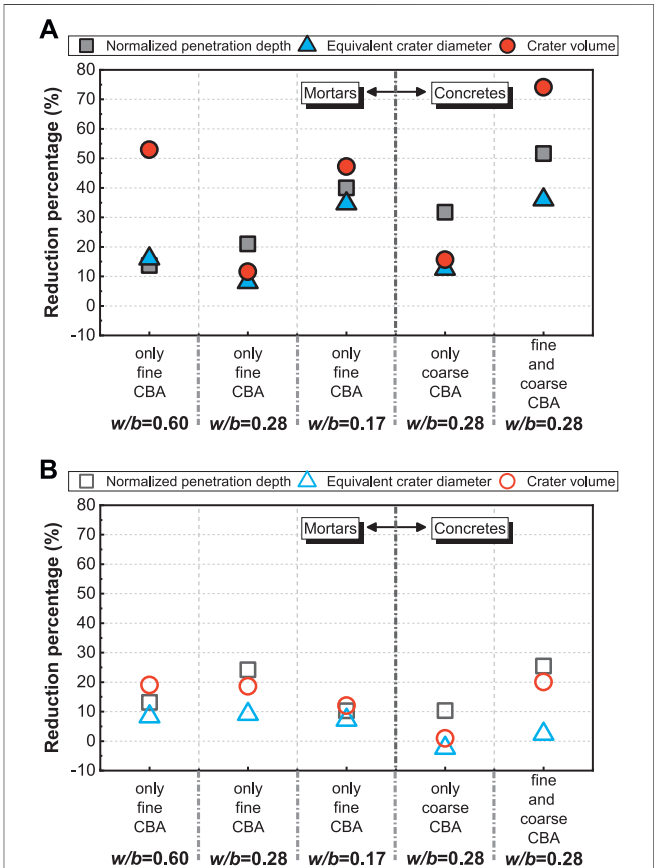

FIGURE 14 | Efficiency of CBA in controlling the damage in cement composites subjected to HVPI using **(A)** copper and **(B)** steel projectiles.

the micro-crack propagation under impact loading. In addition, it was reported by Quek et al. (2010) that CBA has higher energy absorption capacity in comparison to GA when crushed during impact. Larger amount of kinetic energy of the penetrating projectile is absorbed by the crush of CBA, leaving less energy available for the process of penetration. Consequently, significantly improved resistance to HVPI in terms of the DOP was observed. Another explanation is the additional friction between the penetrating projectile and CBA which also dissipates the impact energy as experimentally confirmed by (Zhang et al., 2020a).

The visually observed damages to the deformable projectiles as shown in **Figure 4** are qualitative evidences to the aforementioned mechanisms contributing to the reduced DOP due to the presence of CBA. It is further quantified by examining the retrieved projectiles in terms of the length reduction, diameter increase, and mass loss as illustrated in **Figures 9–11**, respectively. As shown in **Figure 9**, the inclusion of fine CBA in mortars (M-0.60-B, M-0.28-B, and M-0.17-B) leads to the higher projectile length reduction by 35–200% in comparison to the counterparts using

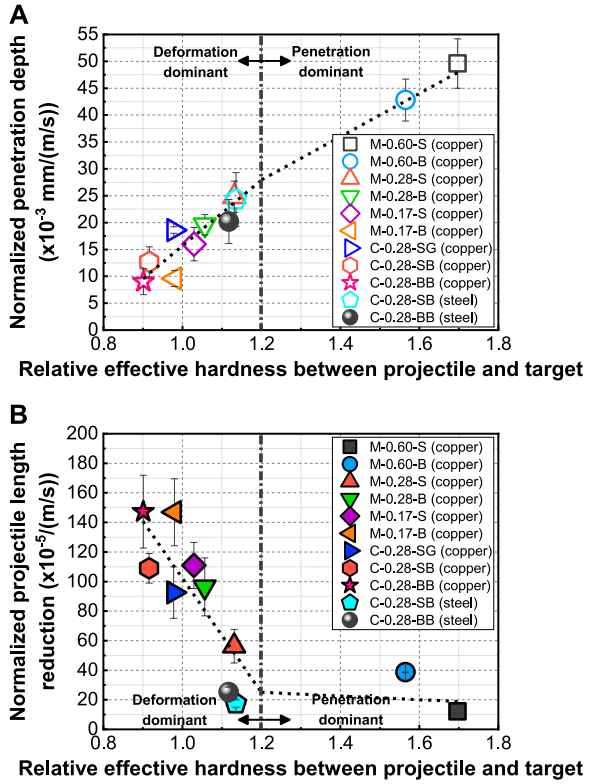

FIGURE 15 | Variation of **(A)** the normalized DOP and **(B)** the projectile length reduction with respect to the REH.

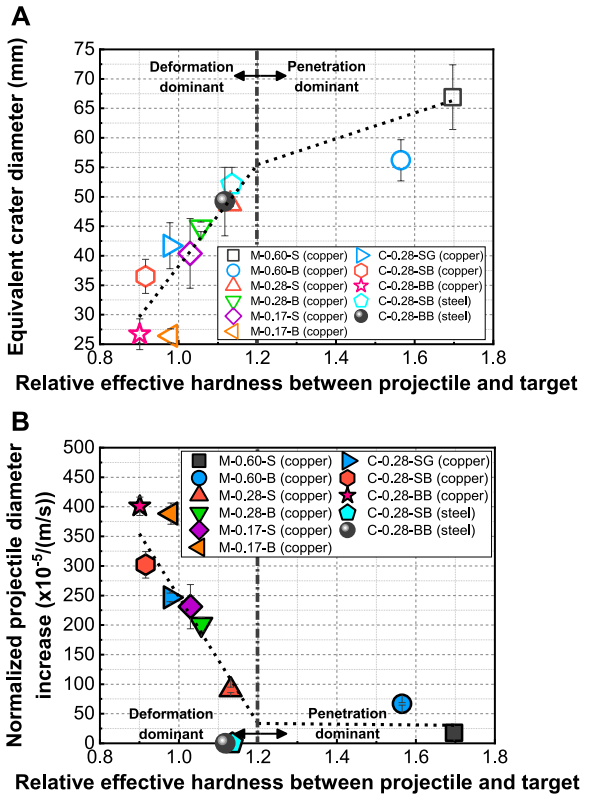

FIGURE 16 | Variation of **(A)** the CD and **(B)** the projectile diameter increase with respect to the REH.

siliceous sand (M-0.60-S, M-0.28-S, and M-0.17-S). The incorporation of coarse CBA in concrete (C-0.28-SB) increases the projectile length reduction by about 20% compared to those using coarse GA (C-0.28-SG). The combined incorporation of both fine and coarse CBA in concrete (C-0.28-BB) leads to 60% and 35% increase of projectile length reduction compared to the concretes without CBA (C-0.28-SG) or with coarse CBA only (C-0.28-SB), respectively. The normalized changes in the diameter and mass for the retrieved projectiles are presented in **Figures 10** and **11**, respectively. More severe increase in the diameter and mass loss was observed for projectiles striking against the mixtures with either fine or coarse CBA alone and their combination. The trends in the damage characteristics of the retrieved projectiles are consistent with the DOPs and supports the mechanisms discussed in the previous paragraph.

Effect of CBA on the Equivalent Crater Diameter

Incorporation of either fine or coarse CBA alone or their combination is also effective in controlling the CD but to a lower extent compared to its influence on the DOP. As observed in **Figure 12**, there is an 8–35% reduction in the CDs for mortars incorporating fine CBA (M-0.60-B, M-0.28-B, and M-0.17-B) compared to those using siliceous sand (M-0.60-S, M-0.28-S, and M-0.17-S). The reduction in CD is 12% for concretes using coarse CBA (C-0.28-SB) compared to the counterpart incorporating coarse GA (C-0.28-SG). The combined incorporation of both fine and coarse CBA in concrete (C-0.28-BB) results in a 36% and 26% reduction of the CD compared to those containing no CBA (C-0.28-SG) or coarse CBA only (C-0.28-SB), respectively. The significantly higher compressive strength and energy absorption capacity of CBA could act as barriers to crack propagation during HVPI as discussed in *Effect of CBA on the Depth of Penetration*. Therefore, smaller CDs were observed. The reduced CDs could also be explained, at least partially, by the deformable nature of the projectiles. Part of the kinetic energy was consumed due to the deformation (**Figures 9–11**) of projectiles themselves or friction between projectiles and CBA (**Figure 4**), resulting in less kinetic energy available for penetration. Consequently, the CDs were reduced.

Effect of CBA on the Crater Volume

Figure 13 illustrates the influence of incorporating CBA on the CV of cement composites subjected to deformable copper HVPI. Using either fine or coarse CBA alone or their combination all results in reduction in CV. The incorporation of fine CBA in mortars (M-0.60-B, M-0.28-B, and M-0.17-B) decreases the CVs by 12–53% in comparison to the counterparts incorporating siliceous sand (M-0.60-S, M-0.28-S, and M-0.17-S). There is a 16% reduction of the CV by replacing coarse GA (C-0.28-SG) with coarse CBA (C-0.28-SB). Furthermore, with the mixed use of both fine and coarse CBA

(C-0.28-BB), a pronounced reduction of 74% was achieved compared to that without any CBA (C-0.28-SG). Since the CV in a cement composite specimen is dependent on its DOP and CD (Zhang, 2020; Zhang et al., 2021b; Zhong et al., 2021), the reduction of CV due to the incorporation of CBA can be expected considering the reduced DOP and CD (see *Effect of CBA on the Depth of Penetration of Cement Composites* and *Effect of CBA on the Equivalent Crater Diameter of Cement Composites*, respectively).

Further Discussion

Efficiency of CBA in Controlling the Different Damage Characteristics of Cement Composites

The efficiency of the incorporation of CBA (both fine and coarse) in controlling the DOP, CD, and CV of cement composites is of great importance for the design of protective structures. The efficiency was unveiled by assessing the percentage reduction of the damage characteristics as presented in **Figures 14A** and **B** for HVPI tests using deformable (copper) and non-deformable (steel) projectiles, respectively. In general, it is more effective in decreasing the DOP and CV than the CD, regardless if fine or coarse CBA alone or their combination were incorporated. However, the most effective approach is the mixed use of fine and coarse CBA which shows the greatest reduction in all damage characteristics. It is also found that the efficiency of CBA in controlling the corresponding damage characteristics of cement composites is different when subjected to deformable (copper) and non-deformable (steel) projectile impact. **Figure 14B** presents the relative reduction of DOP, CD, and CV of the same cement composites tested under the same conditions (e.g., projectile nose shape, diameter, mass, and striking velocities) presented in **Figure 14A** except for the non-deformable nature of the projectiles. By comparing **Figures 14A,B**, it is clear that the beneficial effect of CBA on the resistance of cement composites to HVPI is less significant when struck by the non-deformable (steel) projectile (typically within 20%) compared to that impacted by the deformable (copper) projectile (typically above 20% and up to 80%).

Dependency of the Damage Characteristics of Cement Composites on the Relative Effective Hardness

The experimental study by Zhong et al. (2021) found that the effective hardness and energy absorption capacity under direct tension can be used to characterize the resistance of a variety of advanced cement composites subjected to HVPI in terms of DOP and CV, respectively. Recently, Zhang et al. (2021b) reported a close relationship between DOP and effective hardness for a wide range of cement composites including those utilized CBA and concluded that the reduction of CD and CV could be, at least partially, attributed to the increased splitting tensile strength of cement composites. However, non-deformable projectiles were used in those studies. It is still not clear which material properties can best reflect the contribution of CBA to the resistance of cement composites subjected to HVPI using deformable projectiles. High-intensity pressure is generated at the contact face between a projectile and target upon impact. The penetrating projectile may deform to different extents, depending on the relative properties of the projectile and target as well as the striking velocity (Gold et al., 1996; Xiao et al., 2010; Rakvåg et al., 2013). A part of the projectile kinetic energy can be consumed by the deformation of projectile itself.

It was reported in (Zhang et al., 2020b) that the relative effective hardness (REH) is a good indicator for the actual effect of the competing phenomena of penetration and deformation at a given striking velocity. The REH is defined as the ratio of the effective hardness of projectile to that of cement composites. The hardness values of the copper and steel projectiles provided by the suppliers were determined using HRB and HRC scales, respectively, while the hardness values of the cement composites in this study were measured using HR15T scale following the recommendation in (Callister and Rethwisch, 2012; Zhang et al., 2020a). For consistency, the hardness values of the copper and steel projectiles were also measured using HR15T scale in our laboratory as shown in **Table 3**. Note that the REH is calculated based on the measured hardness values of projectiles and cement composites in terms of HR15T scale.

The variation of the DOP and projectile length reduction with the REH for the deformable projectile impact, including all deformable copper projectiles and some steel projectiles with appreciable deformation (i.e., steel projectiles struck against C-0.28-SB and C-0.28-BB specimens), is presented in **Figure 15**. In general, the DOP increases with the increase of REH, whereas the projectile length reduction generally decreases with the increase of REH. There exists a critical REH of 1.2 beyond which the rate of increase in DOP decreased and the reduction in projectile length dropped significantly. This means that once the effective hardness of the projectile is greater than 1.2 times that of the cement composites, the penetration mechanism is dominant whereas the deformation phenomenon dictates the penetration process when the REH is smaller than this critical value.

The variation of the CD, as well as the projectile diameter increase, with respect to the REH for all deformable copper projectiles and some steel projectiles with appreciable deformation (i.e., steel projectiles struck against C-0.28-SB and C-0.28-BB specimens) is presented in **Figure 16**. Under the given set of impacting conditions, the CD generally increases with the increase of REH, whereas the projectile diameter change generally decreases with the increase of REH. As discussed in *Effect of CBA on the Crater Volume*, since the CV of a target specimen is associated with the DOP and CD (Zhang et al., 2021b), the reduction of CV in cement composites against the impact of deformable projectiles may also be reflected by the reduced REH with the use of CBA.

CONCLUSION

This study provides a systematic experimental investigation on the influence of both fine and coarse calcined bauxite aggregate (CBA) on the resistance of cement composites subjected to deformable projectile impact at a designed velocity of 400 m/s.

Mixtures with Ø100 × 200-mm cylindrical compressive strengths varying between 37.9 and 210.2 MPa were proportioned and subjected to projectile impact. Conical-nosed projectiles made from copper with a purity of 99.5% weighting 7.8 g and possessing a diameter of 8.0 mm were adopted for the projectile impact tests. The damage to a cement composite is quantified based on the depth of penetration (DOP), equivalent crater diameter (CD), and crater volume (CV), while the damage to a projectile is characterized based on the length reduction, diameter increase, and mass loss. The main conclusions are summarized as follows:

1) The use of either fine or coarse CBA improves the resistance of cement composites against deformable projectile impact in terms of the DOP, CD, and CV compared to those using conventional siliceous sand or coarse granite aggregate (GA). The combined use of fine and coarse CBA further reduces the damage characteristics of cement composites compared to the solely use of fine or coarse CBA. The CBA is more effective in decreasing the DOP and CV in comparison to the CD.
2) Replacing of conventional aggregate with CBA causes more severe damage to the deformable projectiles in terms of length reduction, diameter increase, and mass loss. The mixed use of fine and coarse CBA leads to more severe damage to the deformable projectiles compared to those using either fine or coarse CBA alone.
3) The mitigated damage to the cement composites and more severe damage to the deformable projectiles could be explained by the significantly higher compressive strength and energy absorption capacity of CBA. This is also attributable, at least partly, to the friction between the deformable projectile and CBA.
4) The relative effective hardness (REH) between deformable projectile and target is a good indicator for the actual effect of the competing phenomena of penetration and deformation. The penetration mechanism is dominant when the REH is greater than 1.2, whereas the deformation mechanism is dominant when the REH is smaller than 1.2.

DATA AVAILABILITY STATEMENT

The original contributions presented in the study are included in the article, further inquiries can be directed to the corresponding author.

AUTHOR CONTRIBUTIONS

FZ: Formal analysis, Investigation, Writing—original draft. RZ: Formal analysis, Investigation, Writing—review & editing.

ACKNOWLEDGMENTS

The authors appreciate the time and valuable comments from the reviewers that have helped improve the quality of this paper. The authors acknowledge the financial support from the National University of Singapore and Southeast University.

REFERENCES

ASTM C39 (2017). *Standard Test Method for Compressive Strength of Cylindrical Concrete Specimens*. West Conshohocken, PA: ASTM International.

ASTM C127 (2015). *Standard Test Method for Relative Density (Specific Gravity) and Absorption of Coarse Aggregate*. West Conshohocken, PA: ASTM International.

ASTM C469 (2014). *Standard Test Method for Static Modulus of Elasticity and Poisson's Ratio of Concrete in Compression*. West Conshohocken, PA: ASTM International.

Bischoff, P. H., and Perry, S. H. (1991). Compressive Behaviour of Concrete at High Strain Rates. *Mater. Struct.* 24 (6), 425–450. doi:10.1007/bf02472016

Bludau, C., Keuser, M., and Kustermann, A. (2006). Perforation Resistance of High-Strength Concrete Panels. *ACI Struct. J.* 103 (2), 188–195. doi:10.14359/15176

British Standards BS 812-110 (1990). *Testing Aggregates - Part 110: Methods for Determination of Aggregate Crushing Value (ACV)*. London: British Standards Institution.

Cai, Z., Liu, F., Yu, J., Yu, K., and Tian, L. (2021). Development of Ultra-high Ductility Engineered Cementitious Composites as a Novel and Resilient Fireproof Coating. *Construct. Build. Mater.* 288, 123090. doi:10.1016/j.conbuildmat.2021.123090

Callister, W. D., Jr, and Rethwisch, D. G. (2012). *Fundamentals of Materials Science and Engineering: An Integrated Approach*. Fourth Edition ed. Hoboken, NJ, USA: John Wiley & Sons.

Dancygier, A. N., and Yankelevsky, D. Z. (1999). Effects of Reinforced Concrete Properties on Resistance to Hard Projectile Impact. *ACI Struct. J.* 96 (2), 259–269.

Dancygier, A. N., Yankelevsky, D. Z., and Jaegermann, C. (2007). Response of High Performance Concrete Plates to Impact of Non-deforming Projectiles. *Int. J. Impact Eng.* 34 (11), 1768–1779. doi:10.1016/j.ijimpeng.2006.09.094

Feng, J., Song, M., Sun, W., Wang, L., Li, W., and Li, W. (2018). Thick Plain Concrete Targets Subjected to High Speed Penetration of 30CrMnSiNi2A Steel Projectiles: Tests and Analyses. *Int. J. Impact Eng.* 122, 305–317. doi:10.1016/j.ijimpeng.2018.09.005

Gold, V. M., Vradis, G. C., and Pearson, J. C. (1996). Concrete Penetration by Eroding Projectiles: Experiments and Analysis. *J. Eng. Mech.* 122 (2), 145–152. doi:10.1061/(asce)0733-9399(1996)122:2(145)

Gomez, J. T., and Shukla, A. (2001). Multiple Impact Penetration of Semi-infinite Concrete. *Int. J. Impact Eng.* 25 (10), 965–979. doi:10.1016/s0734-743x(01)00029-x

Kœchlin, P., and Potapov, S. (2009). Classification of Soft and Hard Impacts—Application to Aircraft Crash. *Nucl. Eng. Des.* 239 (4), 613–618. doi:10.1016/j.nucengdes.2008.10.016

Kong, X. Z., Wu, H., Fang, Q., Zhang, W., and Xiao, Y. K. (2017). Projectile Penetration into Mortar Targets with a Broad Range of Striking Velocities: Test and Analyses. *Int. J. Impact Eng.* 106, 18–29. doi:10.1016/j.ijimpeng.2017.02.022

Li, Q. M., Reid, S. R., Wen, H. M., and Telford, A. R. (2005). Local Impact Effects of Hard Missiles on Concrete Targets. *Int. J. Impact Eng.* 32 (1), 224–284. doi:10.1016/j.ijimpeng.2005.04.005

Maalej, M., Quek, S. T., and Zhang, J. (2005). Behavior of Hybrid-Fiber Engineered Cementitious Composites Subjected to Dynamic Tensile Loading and Projectile Impact. *J. Mater. Civ. Eng.* 17 (2), 143–152. doi:10.1061/(asce)0899-1561(2005)17:2(143)

Máca, P., Sovják, R., and Konvalinka, P. (2014). Mix Design of UHPFRC and its Response to Projectile Impact. *Int. J. Impact Eng.* 63, 158–163. doi:10.1016/j.ijimpeng.2013.08.003

Nia, A. A., Zolfaghari, M., Khodarahmi, H., Nili, M., and Gorbankhani, A. H. (2014). High Velocity Penetration of Concrete Targets with Eroding Long- Rod

Projectiles; an Experiment and Analysis. *Int. J. Prot. Struct.* 5 (1), 47–63. doi:10.1260/2041-4196.5.1.47

Ohno, T., Uchida, T., Matsumoto, N., and Takahashi, Y. (1992). Local Damage of Reinforced Concrete Slabs by Impact of Deformable Projectiles. *Nucl. Eng. Des.* 138 (1), 45–52. doi:10.1016/0029-5493(92)90277-3

Peng, Y., Wu, H., Fang, Q., Liu, J. Z., and Gong, Z. M. (2016). Impact Resistance of Basalt Aggregated UHP-SFRC/fabric Composite Panel against Small Caliber Arm. *Int. J. Impact Eng.* 88, 201–213. doi:10.1016/j.ijimpeng.2015.10.011

Quek, S. T., Lin, V. W. J., and Maalej, M. (2010). Development of Functionally-Graded Cementitious Panel against High-Velocity Small Projectile Impact. *Int. J. Impact Eng.* 37, 928–941. doi:10.1016/j.ijimpeng.2010.02.002

Rakvåg, K. G., Børvik, T., Westermann, I., and Hopperstad, O. S. (2013). An Experimental Study on the Deformation and Fracture Modes of Steel Projectiles during Impact. *Mater. Des.* 51, 242–256. doi:10.1016/j.matdes.2013.04.036

Riedel, W., Nöldgen, M., Straßburger, E., Thoma, K., and Fehling, E. (2010). Local Damage to Ultra High Performance Concrete Structures Caused by an Impact of Aircraft Engine Missiles. *Nucl. Eng. Des.* 240 (10), 2633–2642. doi:10.1016/j.nucengdes.2010.07.036

Song, D., Tan, Q., Zhan, H., Liu, F., and Jiang, Z. (2019). Experimental Investigation on the Cellular Steel-Tube-Confined Concrete Targets against Projectile Impact. *Int. J. Impact Eng.* 131, 94–110. doi:10.1016/j.ijimpeng.2019.05.004

Wang, S., Le, H. T. N., Poh, L. H., Feng, H., and Zhang, M.-H. (2016). Resistance of High-Performance Fiber-Reinforced Cement Composites against High-Velocity Projectile Impact. *Int. J. Impact Eng.* 95, 89–104. doi:10.1016/j.ijimpeng.2016.04.013

Werner, S., Thienel, K.-C., and Kustermann, A. (2013). Study of Fractured Surfaces of Concrete Caused by Projectile Impact. *Int. J. Impact Eng.* 52, 23–27. doi:10.1016/j.ijimpeng.2012.09.005

Wu, H., Fang, Q., Chen, X. W., Gong, Z. M., and Liu, J. Z. (2015). Projectile Penetration of Ultra-high Performance Cement Based Composites at 510-1320 m/s. *Construct. Build. Mater.* 74, 188–200. doi:10.1016/j.conbuildmat.2014.10.041

Wu, H., Fang, Q., Gong, J., Liu, J. Z., Zhang, J. H., and Gong, Z. M. (2015). Projectile Impact Resistance of Corundum Aggregated UHP-SFRC. *Int. J. Impact Eng.* 84, 38–53. doi:10.1016/j.ijimpeng.2015.05.007

Wu, Z., Zhang, J., Fang, Q., Yu, H., and Haiyan, M. (2021). Mesoscopic Modelling of Concrete Material under Static and Dynamic Loadings: A Review. *Construct. Build. Mater.* 278, 122419. doi:10.1016/j.conbuildmat.2021.122419

Wu, Z., Zhang, J., Yu, H., and Ma, H. (2020). 3D Mesoscopic Investigation of the Specimen Aspect-Ratio Effect on the Compressive Behavior of Coral Aggregate concrete. *Compos. B. Eng.* 198, 108025. doi:10.1016/j.compositesb.2020.108025

Wu, Z., Zhang, J., Yu, H., Ma, H., Chen, L., Dong, W., et al. (2020). Coupling Effect of Strain Rate and Specimen Size on the Compressive Properties of Coral Aggregate concrete: A 3D Mesoscopic Study. *Compos. B. Eng.* 200, 108299. doi:10.1016/j.compositesb.2020.108299

Xiao, X., Zhang, W., Wei, G., and Mu, Z. (2010). Effect of Projectile Hardness on Deformation and Fracture Behavior in the Taylor Impact Test. *Mater. Des.* 31 (10), 4913–4920. doi:10.1016/j.matdes.2010.05.027

Yankelevsky, D. Z. (2017). Resistance of a Concrete Target to Penetration of a Rigid Projectile - Revisited. *Int. J. Impact Eng.* 106, 30–43. doi:10.1016/j.ijimpeng.2017.02.021

Zhang, F., Poh, L. H., and Zhang, M.-H. (2020). Critical Parameters for the Penetration Depth in Cement-Based Materials Subjected to Small Caliber Non-deformable Projectile Impact. *Int. J. Impact Eng.* 137, 103471. doi:10.1016/j.ijimpeng.2019.103471

Zhang, F., Poh, L. H., and Zhang, M.-H. (2021). Effect of Bauxite Aggregate in Cement Composites on Mechanical Properties and Resistance against High-Velocity Projectile Impact. *Cem. Concr. Compos.* 118, 103915. doi:10.1016/j.cemconcomp.2020.103915

Zhang, F., Poh, L. H., and Zhang, M.-H. (2020). Resistance of Cement-Based Materials against High-Velocity Small Caliber Deformable Projectile Impact. *Int. J. Impact Eng.* 144, 103629. doi:10.1016/j.ijimpeng.2020.103629

Zhang, F. (2020). Resistance of Cement-Based Materials against High-Velocity Projectile Impact. Ph.D. thesis. Singapore: National University of Singapore.

Zhang, F., and Zhong, R. (2021). A Parametric Study on the High-Velocity Projectile Impact Resistance of UHPC Using the Modified K&C Model. *J. Build. Eng.*, 103514. doi:10.1016/j.jobe.2021.103514

Zhang, J., Chen, C., Li, X., Chen, X., and Zhang, Y. (2021). Dynamic Mechanical Properties of Self-Compacting Rubberized Concrete under High Strain Rates. *J. Mater. Civ. Eng.* 33 (2), 04020458. doi:10.1061/(asce)mt.1943-5533.0003560

Zhang, M. H., Shim, V. P. W., Lu, G., and Chew, C. W. (2005). Resistance of High-Strength Concrete to Projectile Impact. *Int. J. Impact Eng.* 31 (7), 825–841. doi:10.1016/j.ijimpeng.2004.04.009

Zhang, T., Wu, H., Huang, T., Sheng, J. H., Fang, Q., and Zhang, F. J. (2018). Penetration Depth of RC Panels Subjected to the Impact of Aircraft Engine Missiles. *Nucl. Eng. Des.* 335, 44–53. doi:10.1016/j.nucengdes.2018.04.025

Zhong, R., Zhang, F., Poh, L. H., Wang, S., Le, H. T. N., and Zhang, M.-H. (2021). Assessing the Effectiveness of UHPFRC, FRHSC and ECC against High Velocity Projectile Impact. *Cem. Concr. Compos.* 120, 104013. doi:10.1016/j.cemconcomp.2021.104013

Zielinski, A. (1984). Fracture of Concrete under Impact Loading. *Struct. Impact Crashworthiness* 2, 654–665.

Conflict of Interest: The authors declare that the research was conducted in the absence of any commercial or financial relationships that could be construed as a potential conflict of interest.

Publisher's Note: All claims expressed in this article are solely those of the authors and do not necessarily represent those of their affiliated organizations, or those of the publisher, the editors and the reviewers. Any product that may be evaluated in this article, or claim that may be made by its manufacturer, is not guaranteed or endorsed by the publisher.